Journal of
Stem Cell Research & Therapy
ISSN: 2157-7633

Tokalov et al., J Stem Cell Res Ther 2016, 6:8
DOI: 10.4172/2157-7633.1000350

Research Article Open Access

Advanced Model for Evaluation of iPSCs Lung Engraftment

Tokalov SV[1], Fleischer A[1] and Bachiller D[1,2]*

[1]*Fundación Caubet-Cimera, Development and Regeneration Program, Spain*
[2]*Consejo Superior de Investigaciones Científicas (CSIC), Spain*

Abstract

Induced Pluripotent Stem Cells (iPSCs) based regenerative medicine offers new opportunities for the treatment of a number of pathologies affecting different organs, including the lung. One of the main challenges affecting iPSCs based therapies is the low level of iPSCs engraftment. While the exact mechanisms by which systemically administrated iPSC might be recruited to lung remain poorly understood recent results show that their ability to engraft might not solely be a property of iPSC but might be caused by some events in recipients' lungs, including modifications of some signaling pathways due to damage, repair or developmental processes.

Engraftment of Infrared Fluorescent Protein (iRFP) expressing iPSCs (iRFP-iPSCs) into intact and damaged lung was investigated 2 weeks after hemithorax (HTI, right lung) irradiation with 0 (sham treated control), 10 and 20 Gy, or after intratracheal administration of bleomycin (BLM, 0.075U) to 8 weeks old mice and 1 day old intact pups. Location of iRFP-iPSCs was recorded *in vivo*, *ex vivo* during autopsy, in the dissected organs and in tissue sections 1 day and 1 week after iRFP-iPSCs administration.

Increased enrollment of single iRFP-iPSCs into the both HTI and BLM challenged lungs was detected *ex vivo* and in the dissected organs and was also confirmed by histological examinations shortly after administration, but did not increase in time. In contrast, injection of iRFP-iPSCs to 1 day old intact pups allowed for robust lung uptake, as well as for the development of donor-derived iRFP-iPSCs colonies in lung, as was revealed 1 week after their transplantation.

One day old pups represent an useful model in which to analyze iPSCs capture and engraftment in the lung.

Keywords: Regenerative medicine; Bleomycin; Intratracheal; Pulmonary pathologies; Lung malfunction

Introduction

Pulmonary pathologies are one of the most common causes of death in human populations. Lung malfunction can be caused by many different conditions from preterm delivery (developmental lung abnormalities) and hereditary diseases (cystic fibrosis) to chronic inflammatory processes, malignant transformations in the respiratory system (lung cancer), ionizing radiation (radiotherapy) and certain antibiotics (chemotherapy) and so on.

Preterm birth occurs in approximately 10% of human pregnancies between 20 and 37 weeks of gestation [1]. The resulting developmental lung abnormalities are the most common complication in extreme premature infants accounting for more than 70% of perinatal mortality [2]. In spite of recent advances in perinatal care, rates of pulmonary dysplasia have not dramatically changed over recent years [3].

Cystic fibrosis is the most common autosomal recessive disease. It is caused by mutations in the gene encoding the cystic fibrosis transmenbrane conductance regulator –CFTR- [4]. At three months of age, most babies with cystic fibrosis have abnormalities detectable by chest-computed tomography [5]. The average lifespan of cystic fibrosis patients is around 40 years and obviously cystic fibrosis is also the target of novel medications that may alleviate the pulmonary symptoms [6].

Lung cancer is one of the most frequent and the deadlier cancer type [7]. Radiotherapy plays a fundamental role in treating non-small cell lung cancer (NSCLC), which accounts for approximately 80% of all lung cancer cases, but pulmonary injury induced by hemithorax irradiation (HTI) to adjacent normal lung tissue is a big dose-limiting factors [8] and chemotherapy administration often even increases the risk of radiation pneumonitis in radio-chemotherapy of advanced NSCLC [9]. The overall 2-year survival for patients remains low and the disease still is a serious clinical challenge [10].

Developing new treatments for lung malfunction is therefore, of paramount importance. Recently, the potential use of induced pluripotent stem cells (iPSCs) to regenerate injured lungs and repair the alveolar epithelium has attracted increasing interest [11-17]. The *in vivo* study of transplanted iPSCs, and the ultimate feasibility of cell transplantation therapy required the development of novel imaging techniques to longitudinally monitoring of iPSCs localization, proliferation, integration, and differentiation in living subjects [18]. Direct labeling of cells with image tags (e.g. magnetic nanoparticles, fluorescent dyes, quantum dots, radioactive compounds, etc.) had evident disadvantage for *in vivo* imaging of cell proliferation, as the intensity of the signal is halved in each successful cell division [19]. While both luminescent and fluorescent genetically encoded markers escape this obstacle, luciferase readout was complicated *in vivo* by the need for substrate injection and the dependence on endogenous ATP [20]. Fluorescent *in vivo* imaging in the visible part of the spectrum is hampered by the limited penetration of light inside the body, by scattering and by tissue absorption and autofluorescence. Infrared fluorescent proteins iRFP [21], however, mainly overcame these limitations and represent a significant advance for *in vivo* tracking of both cell delivery and proliferation [2,12,13,15].

***Corresponding author:** Bachiller D, Fundación Caubet-Cimera, Development and Regeneration Program, Consejo Superior de Investigaciones Científicas (CSIC), Ctra. Sóller Km 12, 07110 Bunyola (Balearic Islands), Spain, E-mail: bachiller@caubet-cimera.es

Received June 13, 2016; **Accepted** July 04, 2016; **Published** July 14, 2016

Citation: Tokalov SV, Fleischer A, Bachiller D (2016) Advanced Model for Evaluation of iPSCs Lung Engraftment. J Stem Cell Res Ther 6: 350. doi: 10.4172/2157-7633.1000350

One of the main challenges that iPSCs based therapies are facing is the low level of iPSCs enrolment to the target sites. Using iRFP labeled iPSCs (iRFP-iPSCs) it was recently shown that, in spate of a highly significant iRFP-iPSCs enrolment in lung of intact mice, a day later almost all the cells had leaved the lung through the vascular system [12].

Recent results show that iPSCs ability to structurally engraft might not solely be an intrinsic cellular property, but also be caused by some events in the recipient lung, including modifications of some signaling pathways due to damage, recovery, or developmental processes. Several studies have demonstrated that more iPSCs integrated into the target lung after lipopolysaccharide- LPS, [11], high stretch ventilation- HSV, [16], or BLM-induced [13,17] acute lung injury (ALI).

Recovery from ALI is impeded by damage to the integrity of the epithelial barrier, which inhibits alveolar fluid clearance and depletes surfactant [21]. Recent studies of LPS-induced ALI in mouse demonstrated that intravenous delivery of iPSCs attenuated LPS-induced ALI [11], protected mice against HSV-induced lung injury [16] and restored pulmonary function and improved survival in BLM-challenged mice [17]. It has been found that, in addition to their cell-to-cell contact-dependent differentiation capacity, iPSCs modulate the pathophysiological process of lung diseases via secretion of paracrine factors [11,14]. Taken together, iPSCs can suppress ALI [16].

Combining iPSCs ability to engraft into damaged lungs and their capacity to serve as carriers of a therapeutic gene after systemic administration, has a great potential for the treatment of pulmonary pathologies [11], but in contrast to other organs and tissue types such as heart, bone and cartilage, where iPSCs research has already entered the clinical arena, corresponding developments in the respiratory system are only beginning [22]. One of the possibilities to improve these results is to establish a novel animal model allowing iPSCs not only to engraft and differentiate into the lung specific cells but also permitting them to undergo one or even several cell divisions before differentiation to increase cell number at the target site with followed in situ direct reprogramming [23].

The aim of our study is to evaluate the level of engraftment of exogenous iRFP-iPSCs into the lung after systemic administration 2 weeks after HTI with doses of 0 (sham treated control) 10 and 20 Gy, or after intratracheal administration of BLM to 8 weeks old mice and 1 day old intact pups. The results will serve to define an optimal mouse model for the examination of a possible iPSCs role in the treatment of lung pathophysiological processes..

Materials and Methods

Cells

Stable mouse iPSCs were generated in our group (Lorenzo et al., 2013). Cells were cultured on X-Ray inactivated mouse embryonic fibroblast (MEFs) feeder layers. The lines used in this study were stably transfected with an iRFP (λex: 690 nm, λem: 713 nm) expressing construct.

Animals

Athymic and otherwise intact nude male Foxn1nu/nu mice (body weight, 25 ± 1 g), 8 weeks of age were kept at 5 mice per cage. Mice pups were born from C57BL/6J parents. Pregnant mice were kept one per cage. Both strains were received from Harlan (Barcelona, Spain). Mice were fed a common alfalfa-free diet A04 (Scientific Animal Food and Engineering, Barcelona, Spain) with water and food ad libitum and were housed in a room with a 12-hour light-dark cycle for at least one week before experiments. Animal housing and trials were approved by the local animal care committee, according to the institutional guidelines and the national animal welfare regulations.

In vivo and *ex vivo* fluorescent imaging, and histological examination

Non-invasive *in vivo* iRFP imaging of iPSCs location or teratoma formation was performed with a Pearl-Impulse imaging system (LI-COR Biotechnology, Barcelona, Spain), under intraperitoneal ketamin/xilacin anesthesia (K/X) with 120 mg/kg ketamin (Imalgene 1000, Merial, Barcelina, Spain) / 16 mg/kg xilacin (Xilagesic, Calier, Barcelona, Spain). Pearl-Impulse imaging system was calibrated to enable absolute quantification of the fluorescent signal. In this way, longitudinal studies could be compared to those collected earlier and later in the experiment, even over several orders of signal magnitude, without compromising the quantitative results.

Data were acquired and analyzed using the manufacturer's proprietary Pearl-Impulse v1.0 software. Pseudo-color image representing the spatial distribution of photon counts was overlaid with gray-scale light images. At due time, *in vivo* examined mice were euthanized according to approved methods. Whole body and separate organs were inspected for fluorescent emission with the same equipment. In order to estimate the accuracy of the macro-imaging data, to localize more precisely the location of iRFP-iPSCs and to obtain a direct measurement of the of presence of the cells, 10-μm frozen sections of each lung sample were prepared and analyzed by using standard fluorescent microscope (DMI 6000B; Leica Microsystems, Barcelona, Spain). After this, sections were stained with haematoxyline and eosine (HE, Sigma, Barcelona, Spain) and analyzed histologically using the same microscope again.

For immunohistological staining, after permeabilization with 0.1% Triton X-100, the samples were incubated with the primary antibodies overnight at 4°C. The samples were washed with PBS to remove unconjugated primary antibodies. Fluorescein isothiocyanate-labelled secondary antibodies were added and incubated for 2 hrs at 37°C. For genomic DNA staining, samples were incubated with Hoechst33258 and observed under the same fluorescent microscope described above. Nanog, Oct-4, Sox2 and SSEA1 expression were checked to determine iRFP-iPSCs differentiation state.

iRFP-iPSCs IV injection

A total of 1×10^6 iRFP-iPSCs were resuspended in 50 μL of phosphate-buffered saline and administered intravenously into the lateral tail vein of adult mice under intraperitoneal anaesthesia with 120 mg/kg ketamin, (Imalgene 1000, Merial, Barcelina, Spain) / 16 mg/kg xilacin, (Xilagesic, Calier, Barcelona, Spain), or into the retro-orbital sinus of 1 day old pups without anesthesia as described recently. Ten animals per experimental group have been used. Injections were administered with 0.3-mm (30G) needles attached to 0.3-ml insulin syringes (BD Micro-FineTM, Becton Dickinson, Madrid, Spain) under a Leica M50 routine stereo microscope (6.3X-40X, Leica Microsystems, Barcelona, Spain). All manipulations with animals during injections were performed in aseptic surgical conditions.

iRFP-iPSCs teratoma forming potential

An assessment of the tumorigenic capacity of iRFP-iPSCs was carried out using 20 adult mice. To this end 1×106 iRFP-iPSCs in 0.1 ml of phosphate buffer saline were subcutaneously injected into the

subcutis (both lower limbs of each mouse) 2 days after whole body irradiation (WBI). Monitoring of teratoma growth was performed by fluorescence *in vivo* imaging under K/X anesthesia as well as by means of calipers at the same time points since macroscopic tumors were found. Teratoma volume was calculated (width 2×length×0.5). Finally, all mice were sacrificed, teratomas were removed and sections were prepared for histology as described above.

Bleomycin challenged mice

Adult mice were intratracheally injected with 0.075U of bleomycin (BLM, 3.0 units/kg, Calier, Barcelona, Spain) in PBS under K/X anesthesia. 1×10^6 iRFP-iPSCs were suspended in 50 µL of PBS were intravenously injected into the lateral tail vein of mice ander K/X anesthesia two weeks after BLM administration. Two groups of 10 mice were sacrificed on day 1 or 7 after iRFP-iPSCs transplantation. Lungs were collected, analyzed and then tissue sections of each lung were prepared for routine histology as described above.

Hemithorax irradiated mice

60 male mice were divided in 3 groups and underwent hemithorax irradiation (HTI) with doses of 0 (sham treated control) 10 and 20 Gy (dose rate: 2.0 Gy/min) under K/X anesthesia. 1×10^6 iRFP-iPSCs suspended in 50 µL of PBS were intravenously injected into the lateral tail vein of mice under K/X anesthesia two weeks after BLM administration. Three groups of 10 mice were sacrificed on day 1 or 7 after iRFP-iPSCs transplantation. Lungs were collected, analyzed and then tissue sections of each lung were prepared for routine histology as described above.

Radiation source and dosimetry

Radiation exposure was carried out using a commercially available Cabinet X-ray system (Model RX-650, 120 kV, 5 mA, and 0.5 mm aluminum filter, Faxitron X-ray Corp, Wheeling, IL). The dosimetry was performed with using a dosimeter (Keithley 35050A) connected to a calibrated ion chamber (Keithley 96035). The chamber was placed in the radiation field in the vicinity of the detector during x-ray measurements.

MEFs were inactivated by X-Ray irradiation (dose 40 Gy, dose rate of 0.83 Gy/min) according to our published protocol. Whole body irradiation with a 4 Gy dose (dose rate: 2.0 Gy/min) was performed for additional immunosuppression of Foxn1nu/nu mice. To this end mice were placed into plastic cages so that 5 animals were irradiated at the same time. To improve homogeneity of dose rate, plate with animals were rotated during irradiation.

To perform HTI exclusively covering the targeted area, a lead collimator (10 mm thick) with circular aperture 10 mm in diameter and an appropriate animal HTI plate were custom made as described recently [24]. Bi-dimensional (2D) dose distribution was visualized using near tissue equivalent self-developing GAFCHROMIC EBT films (International Specialty Products, NJ, USA) using a standardized protocol. Whole EBT films were imaged at a 7-fold magnification using the light channel of the fluorescence microscope described above. The red channel was extracted for analysis using a narrow band pass filter because EBT has a maximum response to red light at 633 nm [28]. The film images were evaluated by defining an area of interest about 2.0 cm × 2.0 cm at the center of each of the areas exposed to the calibrated doses and measuring the scanner response. Clear dose response with higher resolution of EBT films in the region of lower doses was observed (Figure 1). EBT films were additionally analyzed at a 200-fold magnification (Figure 1, inset) at the same recording conditions. The width of the edge between the areas where the color of the EBT film changed from light to dark did not exceed 0.1 mm. The analysis of 2D dose distributions in the selected areas revealed close agreement with visual examination: after irradiation with dose 20 Gy inhomogeneity of less than 5% was revealed in the field underwent HTI, the accumulated dose in the area outside zone of irradiation protected from HTI did not exceed 20 cGy.

Statistics

The experimental results are expressed as the mean ± standard deviation of several independent experiments. Analysis of variance (ANOVA) was performed.

Results

To track transplanted cell fate in a non-invasive manner, recently established mouse iRFP-iPSCs lines [16] stably expressing iRFP (λex: 690 nm, λem: 713 nm) have been used (Figure 2A). Immunostaining shows that iRFP-iPSCs maintain the expression of the pluripotent markers Nanog, Oct4, Sox2 and SSEA1, suggesting that reporter gene expression does not adversely affect iRFP-iPSC pluripotency. In vitro imaging show that the level of fluorescent signal correlates with iRFP-iPSC number (Figure 2 B).

Twenty mice were injected subcutaneously in both lower limbs with 106 iRFP-iPSC, resulting in 100% tumor growth (40 teratomas) at the injection sites. At the first time point tested, 2 days post injection, no external physical evidence of cell growth was detectable, but *in vivo* fluorescent imaging of the animals (Figure 2C) showed that iRFP fluorescence not only clearly distinguished the exogenous cells from the hosts', but also allowed real-time monitoring of subclinical (e.g. without palpable tumor mass measurable by traditional physical means) teratoma formation when the nodules were still too small to be detected even at necropsy. While this means that their presence at this early stage could not be confirmed either visually or by histological examination, all these tumors were actively growing, for non-invasive imaging showed that the level of fluorescent signals increased rapidly with time at the transplanted sites (data not shown). Within 10 to 12 days, visible macroscopic tumors (1 mm. diameter and above) could be observed at the areas with high level of iRFP fluorescence. From that point on, both caliper and fluorescent measurements were

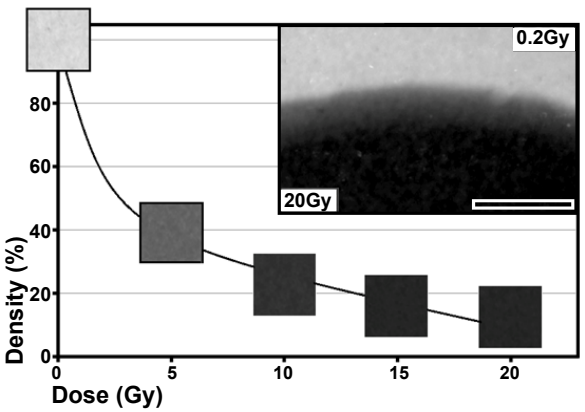

Figure 1: Evaluation of the dose distribution using EBT films. Dose dependent optical density and 2 × 2 cm examples of irradiated EBT films. Microscopic analysis of EBT film after hemithorax irradiation of 1 cm area is shown (inset). Irradiated (20 Gy, dark) and protected (20 cGy, light) areas are clearly separated. Scale Bar:1 mm.

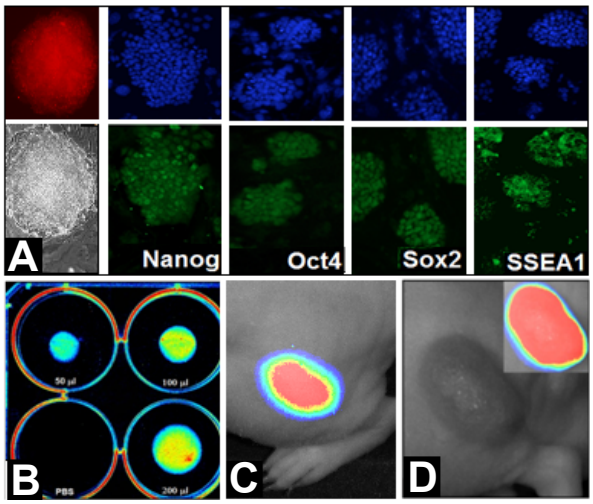

Figure 2: iPSC imaging. A). *In vitro* imaging. Upper left corner, single colony showing IRFP emission. Lower left corner, the same colony in bright field. IRFP-iPSCs colonies were stained with stemness specific antibodies against Nanog, Oct4, Sox2 and SSEA-1 (FITC: bottom). The same colonies show nuclear staining with DAPI, top (B) *In vitro* imaging of different amounts of IRFP-iPSCs. (C) *in vivo* imaging 2 days after iRFP-iPSC subcutaneous injections (no palpable tumors were detectable). (D) Visible teratoma 14 days after injection.

recorded regularly until a humane endpoints was reached (Figure 2D). Once teratomas reached a dimension when they affected the animals' behavior, motility, food and water intake animals were sacrificed and the teratomas removed for analysis.

Histological analysis showed that each mouse had developed tumors with heterogeneous structure. The level of heterogeneity was usually high, with all samples (Figure 3, top left) containing derivatives of the three germ layers, connective tissue (mesoderm, Figure 3A), muscle (mesoderm, Figure 3B), neuronal tissue and pseudostratified epithelium (ectoderm, Figure 3C), gut epithelium in different stages of the development (endoderm, Figure 3D) and hematopoietic tissue (mesoderm, Figure 3E).

iRFP-iPSCs delivery into adult mice

As described in the experimental procedures section, enrolment of the systemically administrated iRFP-iPSCs into damaged lungs of adult animals was analyzed after HTI doses of 0 (sham treated control), 10 and 20 Gy, or after intratracheal administration of BLM (0.075U). To avoid iRFP-iPSCs rejection, immune deficient athymic nude Foxn1nu/nu mice were used. WBI with a 4 Gy dose was performed for additional immune suppression.

No macroscopic pathology was found in control mice during 2 entire periods of examination. These mice usually have some small patches of fur on the back, at the level of the thoracic area (Figure 4A). While no visible changes were found after a single 10 Gy dose of HTI (Figure 4B), HTI with 20 Gy led to hair loss in the irradiated area. The cleared area (10 mm diameter) became detectable on the right part of the mouse breast 2 weeks after a 20 Gy HTI (Figure 4C). 2 weeks after HTI, no significant difference in body weight was detected in 10 Gy irradiated mice in comparison to sham treated controls, but a single irradiation with 20 Gy led to a significant weight loss of 3 ± 1 g on average ($p<0.05$). 2 weeks after BLM administration, mice had a significantly higher weight loss of 5 ± 1 g ($p<0.01$) (Figure 4D). At the same time, no changes in mortality were detected during entire period of examination in all groups of animals.

On day 14 after HTI or BLM exposure, all mice were injected with iRFP-iPSCs (1.0×10^6 in 50 µl of saline) through the tail vein. The Location of iRFP-iPSCs was registered by *ex vivo* fluorescent imaging at 1 day (Figure 4, middle column) and 1 week (Figure 4, right column) after injection. It was found that lung uptake of iRFP-iPSCs was dependent on the time of observation and the treatment applied. In accordance with our previous study no substantial increase of the iRFP fluorescence signal was revealed by organ *ex vivo* imaging, and no significant number of iRFP-iPSCs were observed in the lungs of control mice, both 1 day and 1 week after the transplantation (Figure 4A). In contrast, higher level of iRFP fluorescence was detected during organ *ex vivo* imaging and numerous, isolated iRFP-iPSCs (marked by arrows) were identified in HTI- (Figures 4B and 4C) or BLM-challenged (Figure 4D) lungs 1 day after transplantation (Figure 4, middle column). It is worth mentioning the higher level of iRFP

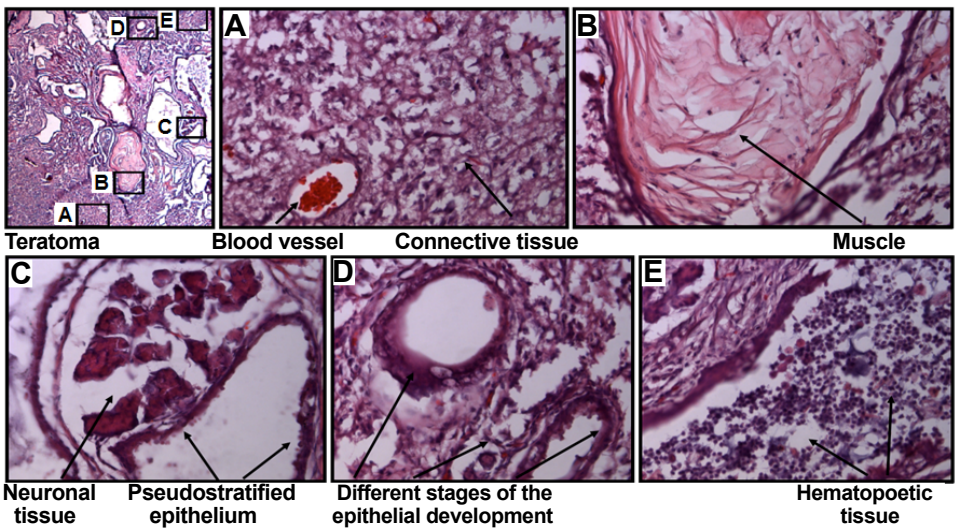

Figure 3: Histological images of iRFP-iPSCs derived teratomas. (A) Vessels interspersed with structures resembling fetal glomeruli (B) Muscle. (C) Rosettes of neural epithelium (D) Epithelial tissues. (E) Hematopoietic tissue.

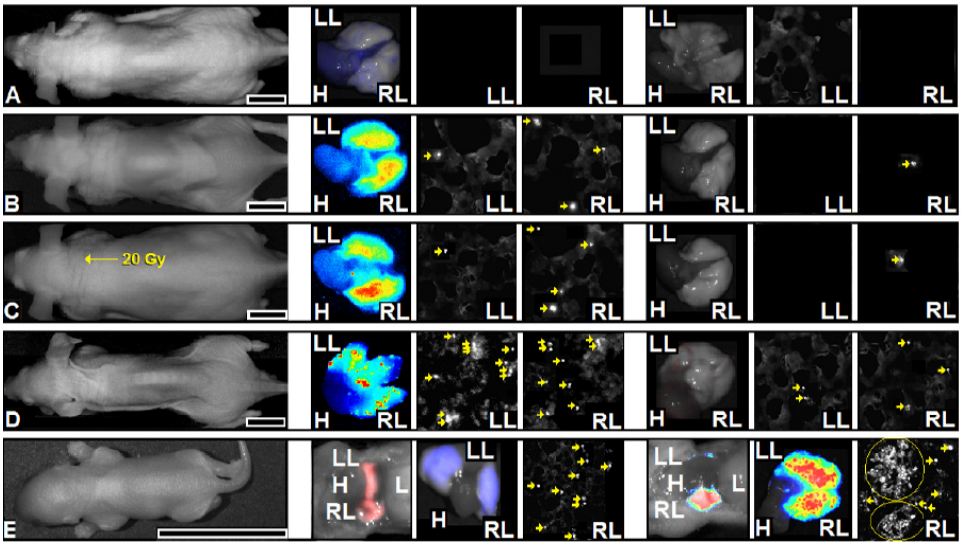

Figure 4: iRFP-iPSCs engraftment after systemic administration. Left column: *In vivo* whole body images of adult mice 2 weeks after HTI with doses of 0 Gy (A), 10 Gy (B), 20 Gy (C), BLM treatment (D), and intact pups (E). Middle and right columns show *ex vivo* images of whole lungs (left lung, LL, right lung, RL) and heart (H) and the corresponding lung sections. Middle column: 1 day after iRFP-iPSCs injection. Right column: 1 week after injection. iRFP-iPSCs abundance in lung and heart is displayed in a color scale proportional to the intensity of the signal. iRFP-iPSCs appearance in sections is noted by arrows. Differences in size of pups reflect the growth occurred between 1 (middle) and 8 (right) days of life. Scale bars correspond to 1 cm.

fluorescence observed by organ *ex vivo* imaging in the irradiated right lobe of lung (RL) in comparison with the protected left lobe of lung (LL) after HTI, both with 10 Gy ($p<0.05$) and 20 Gy ($p<0.001$). In contrast, and as previously described, similar levels of iRFP signal were detected on *ex vivo* organ imaging in the left and right lung lobes of BLM-challenged animals (Figure 4C, middle column). The level of fluorescence in both lungs became negligible 1 week later, although single iRFP-iPSCs were still present (marked by arrows) on tissue sections of HTI and BLM challenged, but not sham treated animals (Figures 4A-4D, right column).

iPSCs engraftment into the lung of 1 day old pups

The engraftment of systemically administrated IRPP-iPSCs into the lung of 1 day old pups was analyzed without any preliminary treatment or immune suppression of the animals. Newborn pups (5-6 animals per litter) were kept together with their mother (1 family per cage). A total of 1×106 iRFP-iPSCs was injected into the retro-orbital sinus of 1 day old pups (Figure 4E, left). No macroscopic pathology was found either in the control or in the experimental groups of pups during the entire period of examination. Animals of the control and experimental groups experienced similar increase in body size (data not shown), indicating the lack of negative effects of iRFP-iPSCs transplantation on early development. In contrast to results obtained with sham treated adult animals, 1 day after iRFP-iPSCs injection in pups a significant increase in the level of fluorescence was shown by *ex vivo* fluorescent imaging at autopsy, on dissected organs, and by the occurrence of single iRFP-iPSCs (marked by arrows) on lung sections (Figure 4E, middle). Contrary to adult animals, 1 week later the level of fluorescence in the lung of pups became significantly higher. It was registered on autopsy, as well as by *ex vivo* fluorescent imaging of separate organs and of frozen lung sections (Figure 4E, right). At this time, not only numerous single iRFP-iPSCs (marked by arrows) but also a significant number of iRFP-iPSCs colonies (noted by circles) were present.

Discussion

Successful reprogramming of somatic cells into iPSCs ushered a new era of regenerative medicine. iPSCs provide powerful new approaches for disease modeling, drug testing, developmental studies, and therapeutic applications. The study of iPSC behavior *in vivo* for the implementation of cell transplantation therapies demands the development of novel imaging techniques for monitoring iPSC localization, proliferation, integration, and differentiation in living objects. Near-infrared-based fluorescence imaging using iRFP gene labeling is a novel technology with potential utility for *in vivo* applications [24]. Here, we expand on our previous results [12,15,13] showing that transplanted iPSCs could be traced *in vivo* with the use of near infrared fluorescent imaging. Importantly, iRFP-iPSCs subcutaneously transplanted into the hind limbs were routinely detected by whole body non-invasive *in vivo* imaging during several days before teratomas became palpable or measurable by traditional physical means. We also show that whole body imaging correlates with organ fluorescence analysis and fluorescent microscopy of frozen sections.

Modern radiotherapy avoids the irradiation of entire organs, concentrating instead in small well-defined areas. In spite of the growing interest in using rodent models for experimental thorax irradiation, specialized radiation sources are still unavailable. The long-standing absence of dedicated systems able to deliver conformal doses to a targeted volume, has led to the design of special radiation units [26,27]. Others modified existing experimental [28,29] or clinical devices that were usually not designed for these purposes. Here, we have used a commercially available X-ray tube with a custom constructed lead collimator with circular aperture, which permits highly localized dose deposition. After irradiation with a 20 Gy dose, the accumulated dose in the area outside the irradiation zone did not exceed 20 cGy, and the width of the edge between irradiated and protected areas did not exceed 0.05 mm (Figure 1).

To better define a possible role of iPSCs in lung restoration, we have performed a series of *in vivo* studies on the time and spatial dynamics of iRFP-iPSCs engraftment into HTI or BLM challenged lungs. By *ex vivo* fluorescent imaging we observed a clear uptake of IRFP-iPSCs in both

BLM and HTI challenged lungs 1 day after their systemic administration and confirmed these findings by histological examination. It has been shown recently that similar single HTI doses were sufficient to induce ALI in mice [30]. However, to our knowledge, the relation of HTI-induced changes in the lung capillaries and lung uptake of systemically administrated iPSCs has not been investigated. Our results provided the first evidence of iPSCs migrating from the systemic circulation to the damaged lung of HTI challenged mice. Notably more iPSCs were registered in the irradiated lung in comparison to the protected one (Figure 4). Similarly, and in agreement with previous publications [13,17], our results show that iPSCs can migrate from systemic circulation to the damaged lung of BLM challenged mice.

It has been shown recently that iPSCs engrafted into the lung after similar conditions of systemic administration, were able to confer some degree of protection from ALI induced by BLM [17], LPS [11,14], or from high stretch ventilation [15], to improve lung function and to increase survival, These findings suggested a role for iPSCs transplantation in lung regeneration therapies. We believe that the effectiveness of iPSCs based therapy could be improved by in situ proliferation of engrafted cells. While no colonies of IRFP-iPSCs were found 1 week in the control, HTI or BLM challenged lungs of adult mice; multiple colonies of IRFP-iPSCs were recorded 1 week after their systemic administration to 1 day old pups. It was shown recently, that rigid fluorescent 2.5 μm microspheres leaved the lung of adult mice 1 day after systemic administration [16,] but had a prolonged stay in the lung of 1 day old pups, probably due to the smaller diameter of the capillary network of the younger animals [31]. These results might help to explain the greater retention of cells by the immature lungs but do not clarify the origin of the colonies. This might be explained by recent findings, suggesting that in mice, a population of special CD71+ cells actively suppresses immune responses in newborns [32]. The process raises their risk of diseases, but it also creates a window during which helpful bacteria can colonize their gut. Weak newborn immune responses allow iPSCs lung colonization without any additional immunosuppression, which suggests that 1-day-old pups might constitute a suitable mouse model for the study of iPSCs lung engraftment.

Another explanation for the different engraftment capacity of iPSCs to lung could simply lie in the use of different injection sites. Interestingly, *in vivo* whole body bioluminescence imaging studies, revealed a strikingly different homing and expansion pattern when T lymphocytes were injected IV or retro-orbitally in a graft versus host diseases model [33]. Similar to our results, these authors observed that cells that were injected through the lateral tail vein migrated directly to the lungs where they failed to expand in the following two weeks. On the contrary, only a small subset of retro-orbitally injected cells trafficked to lungs the day after injection and the majority of cells apparently resided in the retro-orbital sinus cavity [34]. During the next three weeks a strong expansion of cells were observed in different organs, among others the lung. These results are in concordance with our observations concerning retro-orbital injections of iPSCs into newborn mice pups led to a strong accumulation and expansion of iPSCs in the lung after one week of transplantation. Further research in this innovative area will hopefully lead to the realization of cell-based pulmonary therapies [35-39].

In conclusion, by means of a new IRFP expressing iPSC line, we have shown *in vivo* that iPSCs engraftment increases in irradiated or BLM treated adult lungs when compared to non-treated controls. More importantly, we have demonstrated that transplantation into newborn mice improves the engraftment of iRFP-iPSCs into the lung and facilitates the in situ proliferation of the injected cells. These findings illustrate the potential of newborn mouse, in combination with IRFP expression cassettes, as a model for cell transplantation experiments and the study of iPSCs based therapies.

Acknowledgments

We would like to thank Víctor Asensio for his help with the histological analysis of the teratomas.

Funding

Financial support was provided by the European Union (grant number FP7-PEOPLE-2010-IEF); the Spanish Ministry for Science and Innovation (grant numbers PLE2009-0091 IPT-2011-1402-900000 and PI14/01073); and a METROVACESA grant.

Conflict of Interest

The authors have no conflict of interest.

References

1. Firsova AB, Cole TJ, Mollard R (2014) Transient vascular and long-term alveolar deficits following a hyperoxic injury to neonatal mouse lung. BMC Pulm Med 14: 59. [PubMed]
2. Crisanti MC, Koutzaki SH, Mondrinos MJ, Lelkes PI, Finck CM (2008) Novel Methods for Delivery of Cell Based Therapies. J Surg Res 146: 3-10. [PubMed]
3. Fung ME, Thebaud B (2014) Stem cell-based therapy for neonatal lung disease - it's in the juice. Pediatr Res 75: 2-7. [PubMed]
4. Stoltz DA, Meyerholz DK, Welsh MJ (2015) Origins of Cystic Fibrosis Lung Disease N Engl J Med 372: 351-362. [PubMed]
5. Sly PD, Brennan S, Gangell C (2009) Lung disease at diagnosis in infants with cystic fibrosis detected by newborn screening. Am J Respir Crit Care Med 180: 146-52. [PubMed]
6. Becq F (2010) Cystic fibrosis transmembrane conductance regulator modulators for personalized drug treatment of cystic fibrosis: progress to date. Drugs 70: 241-259. [PubMed]
7. Siegel R, Ma J, Zou Z, Jemal A (2014) Cancer statistics, 2014. CA Cancer J Clin 64: 9-29. [PubMed]
8. Moschini I, Dell'Anna C, Losardo PL, Bordi P, D'Abbiero N, et al. (2015) Radiotherapy of non-small-cell lung cancer in the era of EGFR gene mutations and EGF receptor tyrosine kinase inhibitors. Future Oncol 11: 2329-2342. [PubMed]
9. Parashar B, Edwards A, Mehta R, Pasmantier M, Wernicke AG, et al. (2011) Chemotherapy significantly increases the risk of radiation pneumonitis in radiation therapy of advanced lung cancer. Am J Clin Oncol 34: 160-164. [PubMed]
10. Lustberg MB, Edelman MJ (2007) Optimal duration of chemotherapy in advanced non-small cell lung cancer. Curr Treat Options Oncol 8: 38-46. [PubMed]
11. Yang KY, Shih HC, How CK, Chen CY, Hsu HS, et al. (2011) IV delivery of induced pluripotent stem cells attenuates endotoxin-induced acute lung injury in mice. Chest 140: 1243-1253. [PubMed]
12. Tokalov SV, Bachiller D (2012) IV delivery of fluorescent beads. Chest 141: 833-834. [PubMed]
13. Fleischer A, Tokalov SV, Lorenzo IM, Bachiller D (2013) Generation of pure iPS cell-derived endodermal populations for transplantation into mouse models of lung injury, Keystone Symposia, Sagebrush Inn and Conference Center, Taos, New Mexico, USA.
14. Liu YY, Li LF, Yang CT, Lu KH, Huang CC, et al. (2013) Suppressing NF-kB and NKRF pathways by induced pluripotent stem cell therapy in mice with ventilator-induced lung injury. PLoS One 8: e66760. [PubMed]
15. Tokalov SV, Bachiller D (2013) Stem cells based therapy for lung pathologies and blood circulation. TM's 2nd World Molecular and Cell Biology online conference, Bellaire, Texas, USA.
16. Liu YY, Li LF, Fu JY, Kao KC, Huang CC, et al. (2014) Induced Pluripotent Stem Cell Therapy Ameliorates Hyperoxia-Augmented Ventilator-Induced Lung Injury through Suppressing the Src Pathway PLoS ONE 9: e109953. [PubMed]

17. Yan Q, Quan Y, Sun H, Peng X, Zou Z, et al. (2014) A site-specific genetic modification for induction of pluripotency and subsequent isolation of derived lung alveolar epithelial type II cells. Stem Cells 32: 402-413. [PubMed]

18. Cai W, Zhang Y, Kamp TJ (2011) Imaging of induced pluripotent stem cells: from cellular reprogramming to transplantation Am J Nucl Med Mol Imaging 1: 18-28. [PubMed]

19. Tokalov SV, Pieck S, Gutzeit HO (2007) Differences in response to ionization radiation and heat shock exposure in p53 mutated cells. Cell Prolif 40: 24-37.

20. Hock AK, Lee P, Maddocks ODK, Mason SM, Blyth K, et al. (2014) iRFP is a sensitive marker for cell number and tumor growth in high-throughput systems. Cell Cycle 13: 220-226. [PubMed]

21. Hayes M, Curley G, Ansari B, John G, Laffey JG (2012) Clinical review: Stem cell therapies for acute lung injury/acute respiratory distress syndrome – hope or hype. Critical Care 16: 205. [PubMed]

22. Qian L, Huang Y, Spencer CI, Foley A, Vedantham V, et al. (2012) In vivo reprogramming of murine cardiac fibroblasts into induced cardiomyocytes. Nature 485: 593-598. [PubMed]

23. Lorenzo IM, Fleischer A, Bachiller D (2013) Generation of Mouse and Human Induced Pluripotent Stem Cells (iPSC) from Primary Somatic Cells. Stem Cell Rev and Rep 9: 435-450. [PubMed]

24. Filonov GS, Piatkevich KD, Ting LM, Zhang J, Kim K, et al. (2011) Bright and stable near-infrared fluorescent protein for *in vivo* imaging. Nat Biotechnol 29: 757-761. [PubMed]

25. Tokalov SV, Enghardt W, Abolmaali ND (2010) Tumour bed irradiation of human NSCLC tumour xenografts in a nude rat model using common X-ray tube. J Biosci 35: 203-207. [PubMed]

26. Deng H, Kennedy CW, Armour E, Tryggestad E, Ford E, et al. (2007) The small-animal radiation research platform (SARRP): dosimetry of a focused lens system. Phys Med Biol 52**:** 2729-2740. [PubMed]

27. Matinfar M, Ford E, Iordachita I, Wong J, Kazanzides P (2009) Image-guided small animal radiation research platform: calibration of treatment beam alignment. Phys Med Biol 54: 891-905. [PubMed]

28. Graves E, Chatterjiee R, Keall P, Gambhir S, Contag C, et al. (2007) Design and evaluation of a variable aperture collimator for conformal radiotherapy of small animals using a microCT scanner. Med Phys 34 4359-4367. [PubMed]

29. Medina LA, Penilla BIH, Morales MAC, Lopez PG, Jurado R, et al. (2008) Use of an orthovoltage X-ray treatment unit as a radiation research system in a small-animal cancer model. J Exp Clin Cancer Res 27**:** 57. [PubMed]

30. Eldh T, Heinzelmann F, Velalakan A, Budach W, Belka C, et al. (2012) Radiation-induced changes in breathing frequency and lung histology of C57BL/6J mice are time- and dose-dependent. Strahlenther Onkol 188: 274-281. [PubMed]

31. Tokalov SV, Bachiller D (2015) *In vivo* and *post mortem* analysis of fluorescent microsphere distribution in the circulatory network of neonatal and adult mice.

32. Elahi S, Ertelt JM, Kinder JM, Jiang TT, Zhang X, et al. (2013) Immunosuppressive CD711 erythroid cells compromise neonatal host defence against infection. Nature 504: 158. [PubMed]

33. Matamoros S, Leguen CG, Vacon FL, Potel G, Cochetiere MFD (2013) Development of intestinal microbiota in infants and its impact to health. Trends Microbiol 21:167-173. [PubMed]

34. Nervi B, Rettig MP, Ritchey JK, Wang HL, Bauer G, et al. (2007) Factors affecting human T cell engraftment, trafficking, and associated xenogeneic graft-vs-host disease in NOD/SCID beta2mnull mice. Exp Hematol 35: 1823-1838. [PubMed]

35. Quan Y, Wang D (2014) Clinical potentials of human pluripotent stem cells in lung diseases. Clin Transl Med 3: 15. [PubMed]

36. Tokalov SV, Fleischer A, Galves VM, Lorenzo IM, Bachiller D (2012) In vivo Langzeit-Evaluierung der Homing-Eigenschaften induzierter Stammzellen. Experimentalle Strahlentherapie und Klinische Strahlenbiologie 21: 97-101.

37. Tucker SL, Jin H, Wei X, Wang S, Martel MK, et al. (2010) Impact of toxicity grade and scoring system on the relationship between mean lung dose and risk of radiation pneumonitis in a large cohort of patients with non-small cell lung cancer. Int J Radiat Oncol Biol Phys 77: 691-698. [PubMed]

38. Wetsel RA, Wang D, Calame DG (2011) Therapeutic potential of lung epithelial progenitor cells derived from embryonic and induced pluripotent stem cells. Annu Rev Med 62: 95-105. [PubMed]

39. Yardeni T, Eckhaus M, Morris HD, Huizing M, Miller SH (2011) Retro-orbital injections in mice. Lab Anim NY 40: 155-160. [PubMed]